Title

Microbiota configuration determines nutritional immune optimization.

Journal

Proceedings of the National Academy of Sciences, 120(49)

Authors

Han, Seong-Ji
Stacy, Apollo
Corral, Dan
et al.

Publication Date

2023-12-05

DOI

10.1073/pnas.2304905120

Peer reviewed

PNAS RESEARCH ARTICLE | IMMUNOLOGY AND INFLAMMATION

Microbiota configuration determines nutritional immune optimization

Seong-Ji Han[a,1,2], Apollo Stacy[a,3], Dan Corral[a], Verena M. Link[a], Mirian Krystel De Siqueira[b], Liang Chi[a], Ana Teijeiro[a], Daniel S. Yong[a], P. Juliana Perez-Chaparro[a], Nicolas Bouladoux[a], Ai Ing Lim[a,4], Michel Enamorado[a], Yasmine Belkaid[a,5], and Nicholas Collins[a,1,2,5]

Contributed by Yasmine Belkaid; received March 24, 2023; accepted September 25, 2023; reviewed by Christopher A. Hunter and Dennis L. Kasper

Mild or transient dietary restriction (DR) improves many aspects of health and aging. Emerging evidence from us and others has demonstrated that DR also optimizes the development and quality of immune responses. However, the factors and mechanisms involved remain to be elucidated. Here, we propose that DR-induced optimization of immunological memory requires a complex cascade of events involving memory T cells, the intestinal microbiota, and myeloid cells. Our findings suggest that DR enhances the ability of memory T cells to recruit and activate myeloid cells in the context of a secondary infection. Concomitantly, DR promotes the expansion of commensal Bifidobacteria within the large intestine, which produce the short-chain fatty acid acetate. Acetate conditioning of the myeloid compartment during DR enhances the capacity of these cells to kill pathogens. Enhanced host protection during DR is compromised when Bifidobacteria expansion is prevented, indicating that microbiota configuration and function play an important role in determining immune responsiveness to this dietary intervention. Altogether, our study supports the idea that DR induces both memory T cells and the gut microbiota to produce distinct factors that converge on myeloid cells to promote optimal pathogen control. These findings suggest that nutritional cues can promote adaptation and co-operation between multiple immune cells and the gut microbiota, which synergize to optimize immunity and protect the collective metaorganism.

nutrition | memory T cell | microbiota | dietary restriction | metabolites

Significance

Nutrition affects all physiological processes, including those that regulate our immune system. While nutritional interventions demonstrate clinical potential, harnessing nutrition to precisely shape immune responses remains an ongoing challenge. Dietary restriction without undernutrition is a nutritional intervention shown to optimize general health, longevity, and immunity. Here, our work proposes that dietary restriction-mediated optimization of immunological memory requires synergism between the intestinal microbiota, memory T cells, and myeloid cells. These findings have major implications for the design of individually tailored nutritional intervention strategies aimed at preventing and treating disease. Further, the identification of defined microbes as determinants of immune responsiveness to nutritional interventions creates the opportunity to precisely modulate an individual's microbiota to promote optimal therapeutic efficacy.

Nutrition affects all physiological processes, including those that regulate our immune system (1). This established link between nutrition and immunity has created the opportunity to develop therapeutic nutritional interventions that regulate immune responses in various disease states, such as infection, cancer, and chronic inflammatory disorders (2–4). However, while nutritional interventions demonstrate clinical potential, harnessing nutrition to precisely shape immune responses remains an ongoing challenge. A major obstacle in that regard is that human populations show extraordinarily diverse responses to nutritional interventions (5). To uncover the underlying mechanisms by which nutrition regulates immunity at the individual level will greatly improve our ability to design personalized nutritional interventions for the prevention and treatment of disease.

Recent evidence has revealed that fluctuating or reduced dietary intake can positively shape host immunity by enhancing the function of various immune cells (1, 2, 6–8). For instance, we and others have shown that dietary restriction (DR) enhances the function of T cells, which improves host survival in contexts of infection and cancer (6, 7, 9). As mammals evolved throughout periods of food scarcity, these results support the idea that restricted or fluctuating food availability could represent a "beneficial stressor" that promotes optimal host fitness. Consistent with this, DR is associated with numerous physiological health benefits. These include the extension of longevity, improved metabolic profiles and tissue regeneration, as well as the reduction of neurodegeneration, bone loss, cardiovascular disease, and the incidence of cancer (10–19). However, in many settings, the mechanisms remain to be uncovered.

Nutrition can potently regulate host immunity via the microbiota (1, 20). This complex community of microbes is dominantly modulated by host nutrition, and host–microbiota symbiosis is fundamental to sustain organismal fitness and immunity (21, 22). The microbiota possesses a remarkable ability to reconfigure and alter its function in response to physiological alterations, a phenomenon believed to promote host resilience (20, 23–25). For example, restricting dietary intake has been shown to remodel the microbiota in a manner that directly improves host metabolism, prevents cancer, and mitigates aberrant tissue inflammation (9, 26, 27). Based on the closely intertwined relationship between nutrition and the microbiota, commensal adaptation to nutritional fluctuations would be expected to contribute to immune regulation. However, the current relationship with our

[1]Present address: Jill Roberts Institute for Research in Inflammatory Bowel Disease, Joan and Sanford I. Weill Department of Medicine, Department of Medicine, Weill Cornell Medicine, New York, NY 10021.

[2]Present address: Friedman Center for Nutrition and Inflammation, Joan and Sanford I. Weill Department of Medicine, Department of Medicine, Weill Cornell Medicine, New York, NY 10021.

[3]Present address: Department of Cardiovascular and Metabolic Sciences, Lerner Research Institute, Cleveland Clinic, Cleveland, OH 44195.

[4]Present address: Department of Molecular Biology, Princeton University, Princeton, NJ 08544.

[5]To whom correspondence may be addressed. Email: ybelkaid@niaid.nih.gov or nic4015@med.cornell.edu.

This article contains supporting information online at https://www.pnas.org/lookup/suppl/doi:10.1073/pnas.2304905120/-/DCSupplemental.

Published November 27, 2023.

environment and nutrition has drastically deviated from that of our evolutionary history, a phenomenon that has profoundly disrupted the homeostatic host–microbiota symbiosis. For instance, a western diet, which is associated with processed food containing excessive calories and a high content of sugar, fat, salt, and additives, has been shown to shape the host–microbiota relationship toward an aberrant trajectory (23, 28). Further, an unprecedented rise in antibiotic usage is thought to have contributed to a decrease in microbiota diversity and the complete loss of defined taxa (25, 29, 30). Collectively, these nonphysiological pressures have impacted microbiota resilience and, in turn, the hosts' ability to adapt to environmental stressors. This mismatch between the host, its microbiota, and the environment is also believed to have contributed, at least in part, to the dramatic recent rise in autoimmune, heart, allergic, and metabolic diseases (23, 24). Whether this loss of microbiota diversity and resilience also accounts for the ability of specific individuals to positively respond to dietary interventions has not been addressed. More generally, the factors controlling the ability of different individuals to receive immunological benefits from a dietary intervention remain largely unclear.

Here, our work proposes that DR-mediated optimization of host immunity requires synergism between the intestinal microbiota, memory T cells, and myeloid cells. These findings have major implications for the design of individually tailored nutritional intervention strategies aimed at treating and preventing disease.

Results

Microbiota Adaptation to Dietary Restriction Optimizes Immunological Memory. Our previous work demonstrated that DR optimizes the function of circulating memory T cells, which enhanced host protection against secondary infections and tumors (6). It has been shown that animal facilities often harbor a distinct (facility-specific) microbiota that has reduced complexity compared to that of animals raised under physiological or "wild" settings (31–34). To explore whether microbiota configuration dictated immune responsiveness to DR, we assessed the quality of memory responses in separate animal facilities at the NIH (designated Facility A and B). To this end, mice were infected with the attenuated Δ*yopM* mutant of *Yersinia pseudotuberculosis* (*Yptb* Δ*yopM*) via oral gavage (Fig. 1*A*). Under these settings, the pathogen is cleared by day 7 and robust immunological memory is established by 4 wk post-infection (35, 36). At the memory phase, groups of mice remained being fed ad libitum or were placed on 50% DR for 4 wk (which causes approximately 15 to 20% weight loss (6). Mice were then challenged intravenously (i.v.) with the WT strain of *Yptb*, and host protection was assessed 2 d later in the spleen (Fig. 1*A*). Secondary infections were administered i.v. to specifically investigate the role of circulating memory T cells in mediating protection during DR (6). Naive mice that lacked memory cells harbored a similar bacterial burden following *Yptb* infection regardless of nutritional status (Fig. 1*B*). As expected, previously infected (memory) mice fed ad libitum had an improved ability to control the pathogen challenge compared to naive mice (Fig. 1*B*). In line with our previous work, memory mice on DR in Facility A were significantly more protected than memory mice fed ad libitum (6) (Fig. 1*B*). Strikingly, enhanced protection afforded by DR was entirely environment-specific, as genetically identical memory mice (derived from the same breeding barrier as mice in facility A) on DR did not show enhanced protection in Facility B (Fig. 1*C*). These results supported the idea that microbiota composition and/or function dictated immune adaptation and responsiveness to DR.

We next explored whether specific microbes were associated with immune responsiveness to DR by comparing microbiota adaptation in settings where memory responses were enhanced (Facility A) versus not enhanced (Facility B) (Fig. 1 *B* and *C*). Mice fed ad libitum in Facility A had a minor baseline abundance of Bifidobacteriales (0.005%), which increased more than 1,000-fold to constitute 7.4% of the total microbiota during DR (Fig. 1*D* and *SI Appendix*, Fig. S1 *A* and *B*) (37). Interestingly, mice in Facility B had a higher baseline abundance of Bifidobacteriales (2.8%) than mice in Facility A (*SI Appendix*, Fig. S1 *A* and *B*) (37). However, Bifidobacteriales did not significantly increase during DR in Facility B, whereas there was a significant enrichment in Campylobacterales, Desulfovibrionales, and Betaproteobacteriales (Fig. 1*E* and *SI Appendix*, Fig. S1 *A* and *B*) (37). Thus, optimized memory responses during DR were associated with an expansion of Bifidobacteriales.

To establish a role for Bifidobacteriales in optimizing memory responses during DR, we employed a highly controlled system utilizing germ-free (GF) mice colonized with a simplified gut commensal community derived from wild mice, which either lacked or contained Bifidobacteria (Fig. 1*F* and *SI Appendix*, Fig. S1*C*) (37). Mice were first infected with *Yptb* Δ*yopM* and then placed on DR for 4 wk before being reinfected with WT *Yptb* (Fig. 1*F*). In naive mice that did not receive a primary infection, DR with or without Bifidobacteria had no impact on host protection (Fig. 1*F*). DR partially enhanced protective responses in memory mice with the defined microbial community lacking Bifidobacteria (Fig. 1*F*). Critically, memory mice on DR colonized with the community containing Bifidobacteria were significantly better protected than any other group (Fig. 1*F*). Therefore, an enrichment in defined commensal microbes, such as Bifidobacteriales, can promote the optimization of memory responses during DR.

Acetate Optimizes Memory Responses during Dietary Restriction. The microbiota can profoundly regulate host physiology via the production of metabolites, which act both locally and systemically (38). The most abundant microbiota-derived metabolites include the highly immunomodulatory short-chain fatty acids (SCFA) (38). These include acetate, which has been shown to directly enhance both innate and adaptive immune responses (38–40). Thus, gut microbiota-derived metabolites provide a key link between dietary intake and immunoregulation.

Bifidobacteria have the capacity to utilize a broad range of sugars to generate energy, which results in the production of several metabolites, predominantly acetate (39, 41). To explore the possibility that acetate production was enriched during DR, we next utilized shotgun metagenomic sequencing. Indeed, several pathways associated with the production of acetate were enriched in the microbiota of mice on DR (Fig. 2*A*, blue and green) (37). Further, several acetate-related pathways mapped back to Bifidobacteria (e.g., *Bifidobacterium* shunt). Strikingly, there was no enrichment in pathways associated with acetate production in the microbiota of mice in Facility B during DR, or in fact any other functional pathway (Fig. 2*A*) (37). Thus, optimized memory responses during DR are associated with an enrichment in acetate producing Bifidobacteria.

We next performed metabolomics on serum samples to assess systemic SCFA abundance in the setting of DR. Consistent with our metagenomics results, there was a selective increase in acetate in the blood of mice on DR in Facility A (Fig. 2*B*). Acetate can be derived from both the host and the microbiota (42). To discriminate between these sources, we placed SPF (Facility A) and GF mice on DR. Increased acetate in serum was abolished in GF

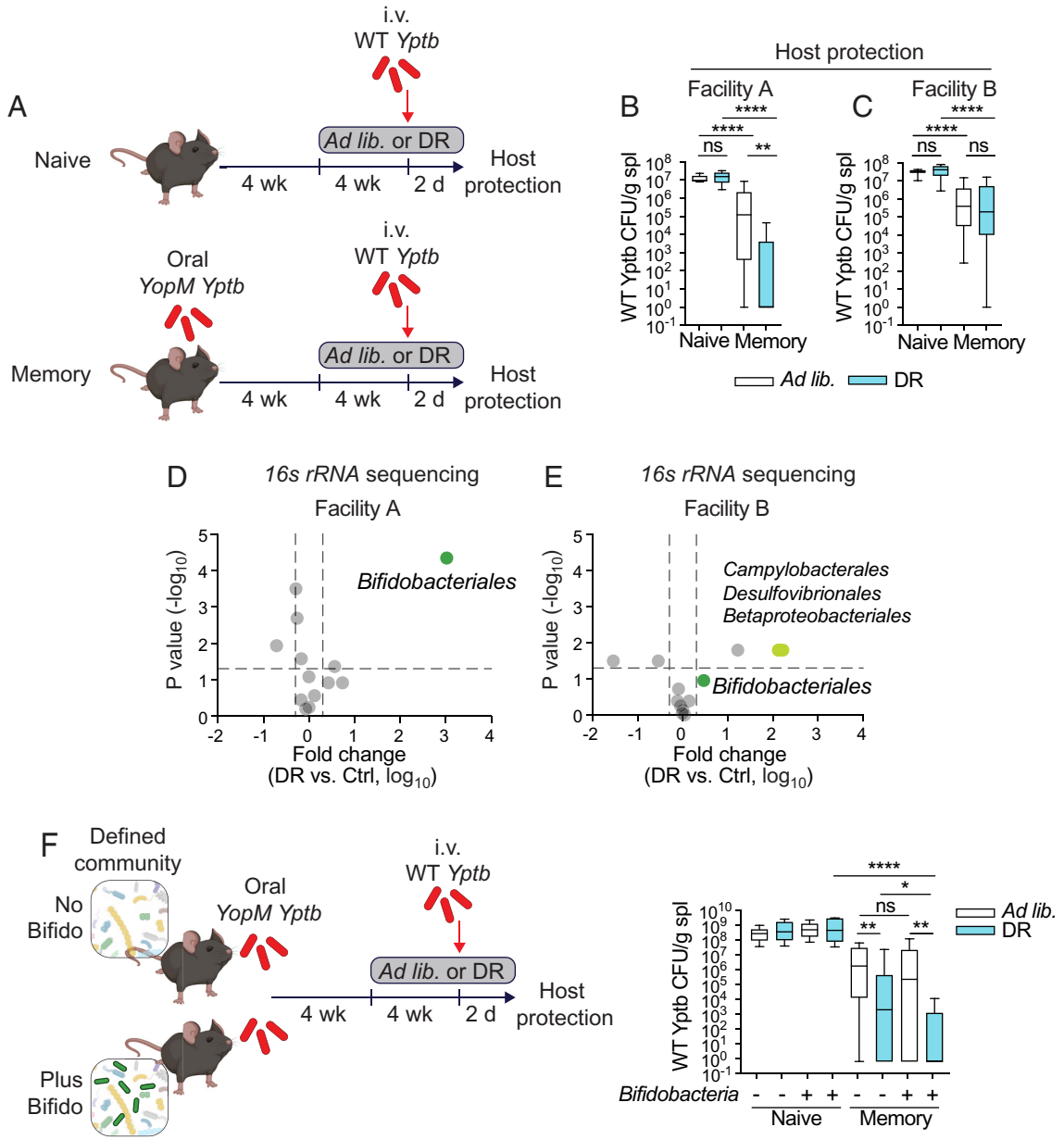

Fig. 1. Microbiota adaptation to dietary restriction optimizes immunological memory. (*A*) Experimental schematic for (*B*) and (*C*). Burden of wild-type *Yptb* in the spleen of naive or previously infected (memory) mice 2 d post challenge in "Facility A" (*B*) and "Facility B" (*C*). *16s rRNA* sequencing on fecal samples of mice fed ad libitum and on DR from "Facility A" (*D*) and "Facility B" (*E*). (*F*) Experimental schematic and burden of wild-type *Yptb* in the spleen of naive and memory mice 2 d post challenge. Pooled from three to five experiments (*B*, *C*, and *F*) or representative of two (*D* and *E*) with three to five mice per group. The line in box and whiskers plots (min to max) represents median (*B*, *C*, and *F*). Ns, not significant, **P* < 0.05, ***P* < 0.01, ****P* < 0.001, *****P* < 0.0001. Mann–Whitney *U* test.

mice on DR (Fig. 2*C*). Therefore, increased acetate observed in response to DR was microbiota-dependent.

To directly test the role of microbiota-derived acetate in optimizing memory responses during DR, we employed a dietary supplementation approach. A major source of SCFA, such as acetate, is gut microbial fermentation of dietary fiber (42). Therefore, following the establishment of immunological memory, mice were placed on isocaloric diets with either high or low levels of fermentable fiber for 4 wk prior to a secondary infection (Fig. 2*D*). Enhanced protection was completely abolished in mice on DR receiving the diet with low fermentable fiber (Fig. 2*D*), suggesting an important role for microbiota-derived SCFA in optimizing immunity in this setting. Further, mice on DR receiving the low fermentable fiber diet supplemented with exogenous acetate showed a partial restoration (approximately 20-fold improved protection) of the response compared to mice on DR receiving a low fermentable fiber diet alone (Fig. 2*D*). Altogether, these data support the idea that microbiota-derived acetate plays an important role in optimizing memory responses during DR.

Enhanced Memory T Cell Function during DR Does Not Require Acetate or Bifidobacteria. Acetate has been shown to promote T cell responses by regulating gene expression, metabolism, and enzyme function (43–46). As our previous results indicated that DR promoted the protective capacity of memory T cells (6), we next focused on memory T cell function and to what degree it was regulated by acetate during DR. To that end, we utilized our recently created *Yptb*-specific transgenic mouse strain containing $CD8^+$ T cells specific for the immunodominant YopE antigen of *Yptb* (YopE-I cells). Naive YopE-I cells were

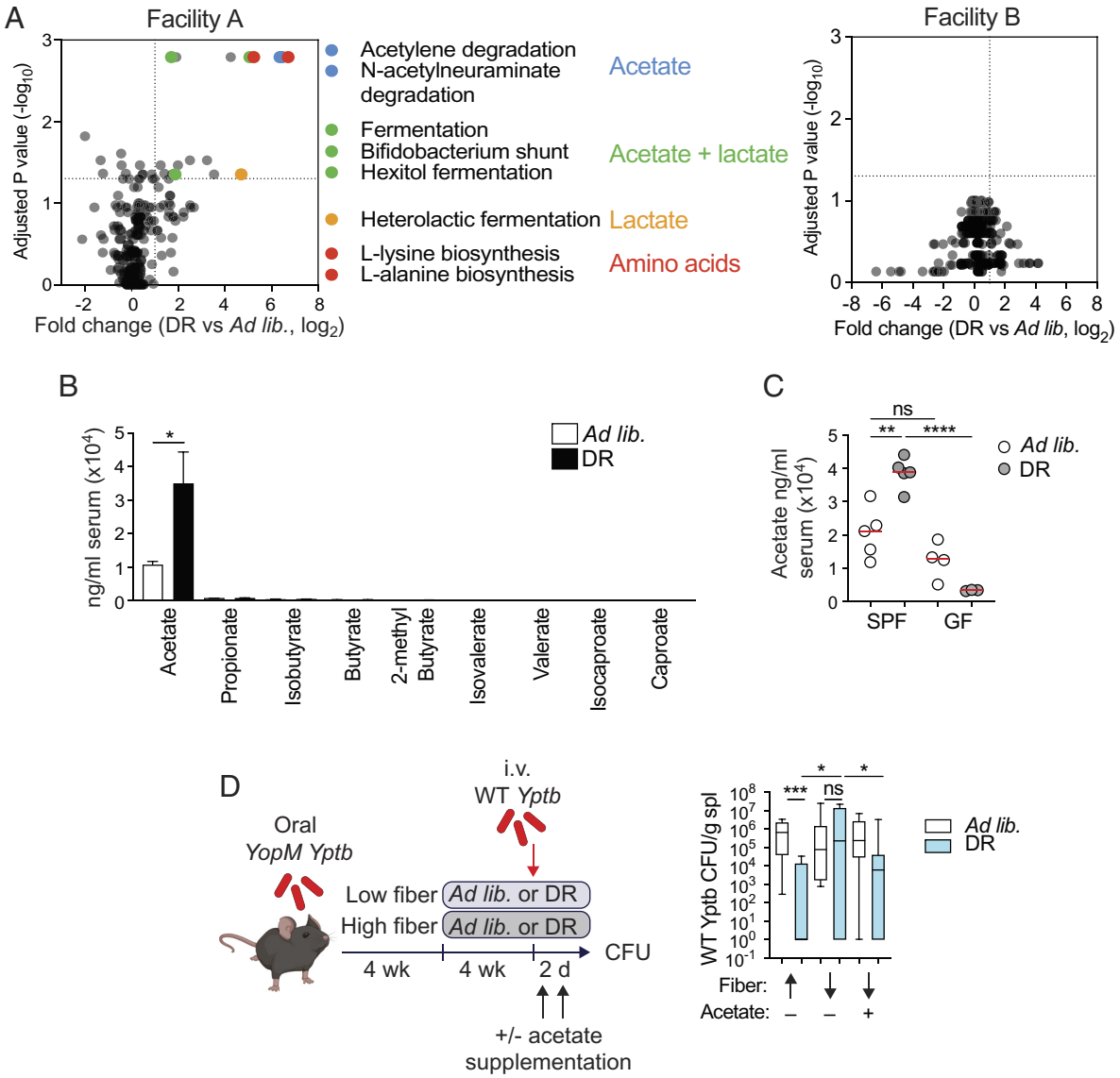

Fig. 2. Acetate optimizes memory responses during dietary restriction. (*A*) Shotgun metagenomics on fecal samples from mice fed ad libitum or on DR for 4 wk from Facilities A and B. (*B*) Metabolomics measuring short-chain fatty acids in serum of mice fed ad libitum or on DR for 4 wk from Facility A. (*C*) Metabolomics measuring acetate in serum of SPF (Facility A) and GF mice fed ad libitum or on DR for 1 wk. (*D*) Experimental schematic and burden of wild-type *Yptb* in the spleen of memory mice (Facility A) 2 d post challenge. Pooled from three experiments (*D*) or representative of two (*A*–*C*) with three to five mice per group. The line represents mean (*C*) or median in box and whiskers plot (min to max) (*D*). Ns, not significant, **P*<0.05, ***P* < 0.01, ****P* < 0.001, *****P* < 0.0001. Mann–Whitney *U* test.

adoptively transferred into WT B6 recipients in Facility A, which then received a primary infection and DR at the memory phase (Fig. 3*A*). First, enhanced protection occurred during DR in Facility A to the same degree regardless of whether mice received YopE-I Tg cells or not (*SI Appendix*, Fig. S2*A*). We found that there was no difference in the frequency of YopE-I cells in the spleen at resting memory or following a secondary challenge during DR (*SI Appendix*, Fig. S2*B*). However, memory T cell function was broadly enhanced during DR, with a higher frequency of YopE-I cells capable of producing IFN-γ and IL-2 following ex vivo restimulation in this setting compared to YopE-I cells from mice fed ad libitum (Fig. 3*B*). Further, of IFN-γ positive YopE-I cells, the mean-fluorescence intensity (MFI) of IFN-γ was higher during DR, indicating a higher production of IFN-γ on a per cell basis (Fig. 3*B*). Enhanced memory T cell function during DR was not limited to cytokine-producing capacity, as a higher proportion of YopE-I cells produced the chemokines CCL3, CCL4, CCL5, and XCL1 in this context (Fig. 3*C*).

To assess the impact of DR on memory T cells at the molecular level, we next performed ATAC-seq on resting circulating memory YopE-I cells from the spleen of mice fed ad libitum or on DR (Fig. 3*D*) (37). We found ~7,000 uniquely accessible chromatin regions in YopE-I cells from mice fed ad libitum and on DR (*SI Appendix*, Fig. S2*C*) (37). Regions of open chromatin were similarly distributed among introns, intergenic regions, exons, and transcription start sites (*SI Appendix*, Fig. S2*D*). Genes with accessible chromatin unique to YopE-I cells from mice on DR related to T cell activation and migration, as determined by pathway analysis (Fig. 3*D* and *SI Appendix*, Fig. S2*E*). This was associated with an enrichment of the transcription factor binding motifs within the genes encoding transcription factor 7 (Tcf-7), the thyroid hormone receptor (Thrb), Gli family zinc finger 2 (Gli2), and growth factor independent 1B (Gfi1b) in regions of accessible chromatin unique to DR (Fig. 3*D*). Thus, consistent with enhanced functional capacity (Fig. 3 *B* and *C*), memory T cells from mice on DR are poised for responsiveness and display enhanced effector potential.

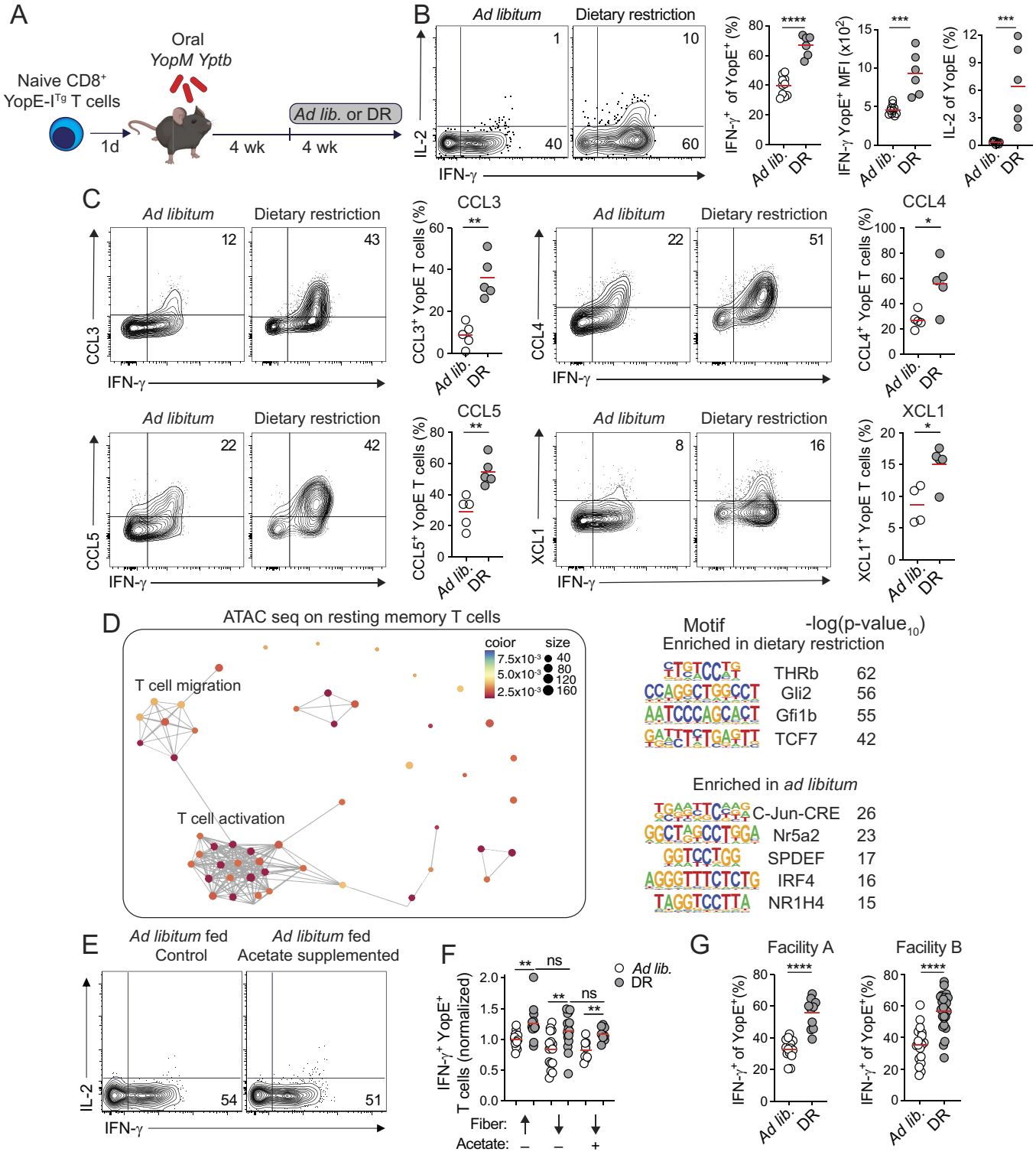

Fig. 3. Enhanced memory T cell responses during DR do not require acetate or Bifidobacteria. (*A*) Experimental schematic for (*B*–*D*). Flow cytometry showing (*B*) IFN-γ, IL-2, (*C*) CCL3, CCL4, CCL5, and XCL1 production by ex vivo stimulated YopE-I cells from the spleen of mice fed ad libitum or on DR. (*D*) ATAC-seq pathway analysis and motif enrichment analysis of resting memory YopE-I cells from the spleen of mice fed ad libitum or on DR. Size of circle reflects the number of genes in the pathway, and color indicates the *P*-value. The line connecting two dots represents sharing of member genes between pathways. Listed pathways were enriched in memory YopE-I cells from mice on DR compared to YopE-I cells from mice fed ad libitum. (*E*) Flow cytometry showing IFN-γ and IL-2 production by ex vivo stimulated YopE-I cells from spleens of control mice fed ad libitum and mice fed ad libitum receiving acetate supplementation. (*F*) IFN-γ production by ex vivo stimulated YopE-I cells from the spleen of mice fed ad libitum or on DR, receiving a diet with or high or low levels of fermentable fiber, with or without acetate supplementation, from Fig. 2*D*. Normalized to the average of the ad libitum group fed a high fiber diet that did not receive acetate in each experiment. (*G*) IFN-γ production by ex vivo stimulated YopE-I cells from spleens of mice fed ad libitum or on DR from "facility A" (Bifidobacteria enriched and enhanced protection during DR) or "facility B" (Bifidobacteria not enriched and no enhanced protection during DR), from Fig. 1 *B* and *C*. Representative of at least three experiments (*B*, *C*, and *E*) or pooled from two to four (*F* and *G*) with three to five mice per group. Pooled from three experiments, each with five mice pooled per group (*D*). The line in graphs represents mean (*B*, *C*, *F*, and *G*). Ns, not significant, **P* < 0.05, ***P* < 0.01, ****P* < 0.001, *****P* < 0.0001. Mann–Whitney *U* test.

Having demonstrated a broad enhancement in the functional capacity of memory T cells from mice on DR, we next assessed the potential role of acetate in this response. Several elegant studies have shown that acetate can directly enhance T cell function (9, 43–46). However, supplementing memory mice fed ad libitum with acetate was not sufficient to enhance memory T cell function (Fig. 3*E*). Further, data in Fig. 2*D* demonstrated that enhanced host protection was abolished during DR in the context of a diet with low fermentable fiber, which was partially restored with acetate supplementation. However, these host protection data did not correlate with memory T cell function, which was enhanced to the same degree during DR, regardless of diet or acetate supplementation (Figs. 2*D* and 3*F*). Similarly, differential host protection observed in distinct animal facilities (Fig. 1 *B* and *C*) did not correlate with memory T cell functional capacity, which was enhanced to the same degree during DR regardless of whether intestinal Bifidobacteriales was enriched or not (Fig. 3*G*). Together, these surprising results supported the idea that enhanced memory T cell responses induced by DR occurred independently of the microbiota and acetate and are not sufficient to mediate enhanced host protection. Importantly, these data also suggest that the cellular target of microbiota-derived acetate is distinct from memory T cells.

Conditioning of the Myeloid Compartment by Acetate and IFNγ Enhances Its Functional Capacity during DR. Optimal killing of pathogens relies on tight co-operation between T cells and the myeloid compartment. Notably, our previous data showed that memory T cells have an increased capacity to produce numerous chemokines and cytokines during DR, which were related to the recruitment and activation of innate immune cells (Fig. 3 *B* and *C*). Further, previous studies have shown that myeloid cells are highly sensitive to DR and that microbiota-derived acetate can regulate the function of myeloid cells (8, 40, 47–50). Therefore, we next assessed the possibility that, in our settings, DR induces memory T cell–derived signals (independently of Bifidobacteria or acetate) that recruit (e.g., chemokines) and prime (e.g., IFN-γ) myeloid cells, which are then boosted in their ability to destroy pathogens by acetate.

Acetate plays a critical role in regulating gene expression via histone acetylation and promoting chromatin accessibility (42). Therefore, we first performed ATAC-seq on myeloid cells from the bone marrow to assess whether acetate was placing these cells in a state poised for protective responses during DR. These analyses demonstrated that both neutrophils and monocytes from memory mice fed ad libitum or on DR were similar in terms of their chromatin accessibility profile (*SI Appendix*, Fig. S3 *A* and *B*) (37). Thus, it was unlikely that acetate was tonically regulating the function of innate cells via an epigenetic mechanism during DR. Rather, it could be that acetate was acting on innate cells to boost their effector capacity as they are in the process of responding to a secondary infection.

In line with increased chemokine production by memory T cells during DR (Fig. 2*C*), we observed increased infiltration by myeloid cells, such as inflammatory monocytes and neutrophils, during a secondary infection in mice on DR (Fig. 4*A*). Transcriptional analysis of myeloid cells in this context suggested that their function was enhanced, as the expression of numerous genes associated with pro-inflammatory immune responses were upregulated in both inflammatory monocytes and neutrophils responding to a secondary infection during DR (Fig. 4*B*) (37). For inflammatory monocytes, genes upregulated during DR included those associated with IFN-γ responsiveness (e.g., *Ifngr1*, *Parp9, Tlr4, Gbp9, Irf1*), pathogen-recognition (e.g., *Cd209e, Clec4e*), inflammation (e.g., *Tlr7, Tlr4, Myd88*), and chemotaxis (e.g., *Cxcr4*, *Fpr*) (Fig. 4*D*). For neutrophils, upregulated genes during DR included those associated with the detection and clearance of pathogens (e.g., *Slc15a2, Irgm1, gbp3, Ifitm1, Clec4e, Cd14, Clec7a*), IFN-γ responsiveness (e.g., *Ifngr1*), and chemotaxis (e.g., *Cxcr3, Cxcr4, Itgb7*) (Fig. 4*E*). Numerous genes were also downregulated, which were similar in both inflammatory monocytes and neutrophils and were associated with fundamental biological processes such as mitosis and spindle formation, not inflammatory processes (Fig. 4 *B* and *C*). Of note, the frequency and activation status of myeloid cells was similar at resting memory in mice fed ad libitum and on DR (*SI Appendix*, Fig. S3 *C* and *D*). Further, the presence of Bifidobacteria promoted myeloid cell accumulation during DR (*SI Appendix*, Fig. S3*E*). These data suggest that both the quantity and quality of myeloid cells were increased in response to a secondary infection during DR.

The above data suggested that myeloid cells had increased responsiveness to IFN-γ and an enhanced ability to infiltrate, accumulate, and uptake pathogens during DR (Fig. 4 *B*–*E*). To establish whether myeloid cells had an enhanced capacity to kill pathogens during DR and whether this process was regulated by the combination of IFN-γ (a memory T cell-derived signal upregulated during DR) and acetate (a microbiota-derived signal upregulated during DR), we performed a gentamycin killing assay (Fig. 4*F*). Myeloid cells from mice fed ad libitum and on DR had a similar ability to kill *Yptb* at baseline (Fig. 4*F*). The ability of myeloid cells to kill *Yptb* was unaffected by the presence of acetate alone (Fig. 4*F*). The presence of IFN-γ alone improved the ability of myeloid cells from mice fed ad libitum and on DR to kill *Yptb*, but to the same degree (Fig. 4*F*). Critically, only myeloid cells from mice on DR showed an increased ability to kill *Yptb* in the presence of both IFN-γ and acetate (Fig. 4*F*). As such, acetate can enhance the functional capacity of myeloid cells during DR, but IFN-γ must be present. Altogether, our results suggest that DR induces a complex cascade of events involving multiple nonredundant signals that optimize memory responses during DR.

Discussion

Here, we present data supporting a model in which DR optimizes immunological memory by simultaneously enhancing the function of memory T cells and the intestinal microbiota, which produce distinct factors that potentially converge on myeloid cells to enhance pathogen control.

Our findings indicate that DR potently remodels the gut microbiota to optimize immunological memory. Modulation of the gut microbiota via diet to regulate immune responses has also been shown in other contexts. For example, a high-fiber diet can enhance immune responses and promote immunotherapy in humans (51, 52). A ketogenic diet has also been shown to modulate the gut microbiota, which impacted gut immune responses (53). Further, it was recently shown that a diet high in fermented food modulates the gut microbiota and systemic immune signatures in humans (54), while low-calorie diets can sensitize tumors to chemotherapy by enhancing immune responses (16, 17). These findings and ours reveal the potential of using a defined nutritional intervention to optimize immune responses to augment traditional therapies (e.g., immune checkpoint blockade, chemotherapy, and radiotherapy). The identification of defined microbes as determinants of immune responsiveness to nutritional interventions also creates the opportunity to precisely modulate an individual's microbiota to promote optimal therapeutic efficacy.

Our findings show that an enrichment in Bifidobacteria optimized memory responses during DR. Bifidobacteria possess a broad

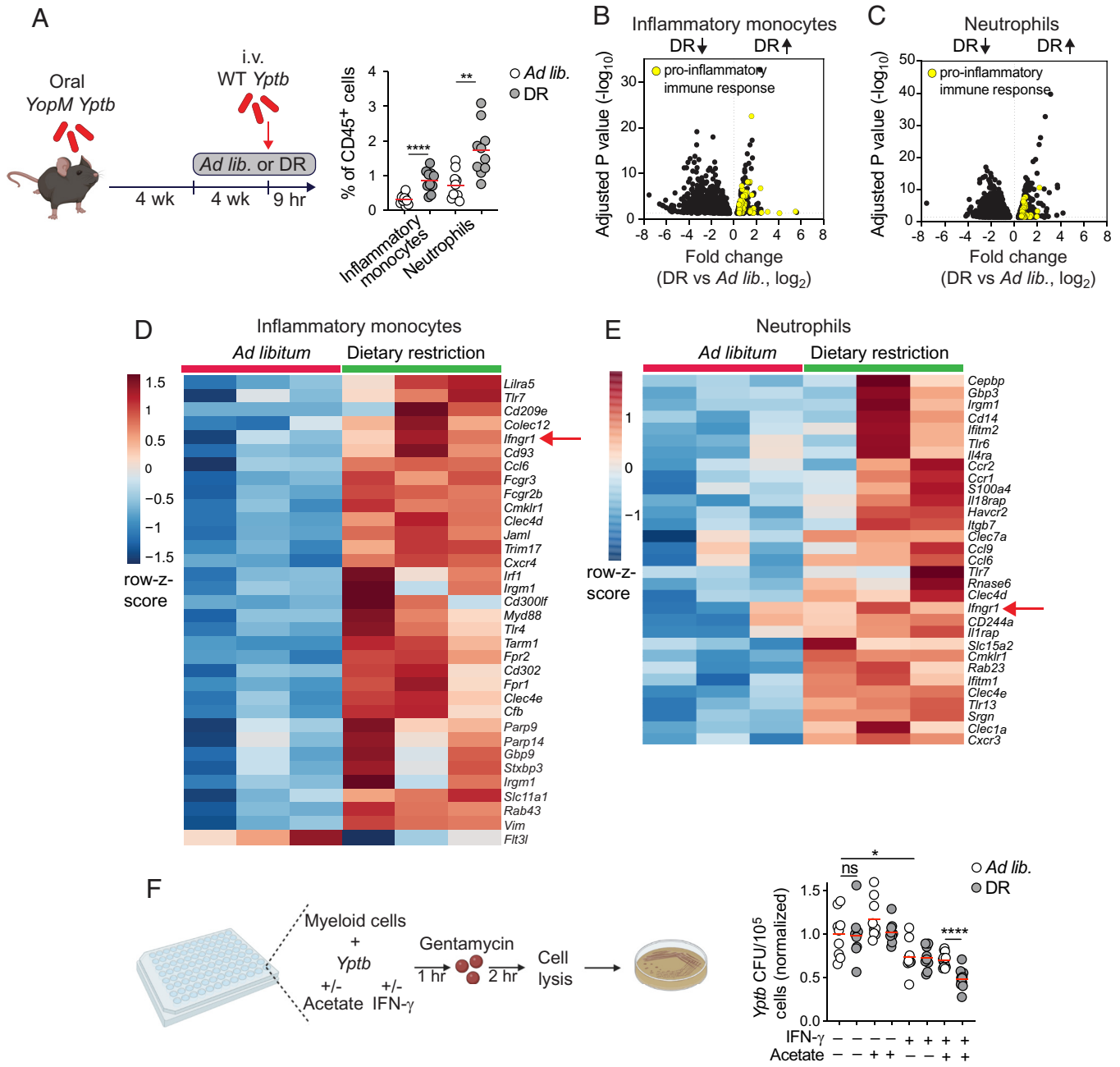

Fig. 4. Conditioning of the myeloid compartment with acetate and IFNγ enhances its killing capacity during DR. (*A*) Experimental schematic for (*A*–*E*). (*A*) Frequency of inflammatory monocytes and neutrophils in the spleen of mice fed ad libitum or on DR at 9 h post a secondary challenge with WT *Yptb*. (*B* and *C*) Volcano plot showing genes differentially expressed in inflammatory monocytes (*B*) and neutrophils (*C*) from spleens of mice fed ad libitum or on DR at 9 h post a secondary challenge with WT *Yptb*. (*D* and *E*) Heatmap showing selected pro-inflammatory immune response genes differentially expressed in (*D*) inflammatory monocytes and (*E*) neutrophils from the spleen of mice fed ad libitum or on DR at 9 h post a secondary challenge with WT *Yptb*. (*F*) Experimental schematic and bacterial burden from the gentamycin killing assay. Each experiment was normalized to the average of the ad libitum fed group that did not receive acetate or IFNγ (*F*). Pooled from two (*A* and *F*) experiments with four to five mice per group. Pooled from three experiments, each with five mice pooled per group (*B*–*E*). The line represents mean (*A* and *F*). Ns, not significant, **P* < 0.05, ***P* < 0.01, ****P* < 0.001, *****P* < 0.0001. Mann–Whitney *U* test.

range of receptors and dedicate significant machinery to the uptake and processing of sugars (55). A major by-product of sugar fermentation by Bifidobacteria is acetate (55). Several studies have demonstrated the ability of Bifidobacteria to promote host protection. Bifidobacteria-derived acetate in particular has been shown to protect the host against gut bacterial toxins and tumors (9, 39, 41). Further, Bifidobacteria is one type of commensal that is sufficient to enhance anti-tumor immunotherapy (anti-PD1) in mouse models via the production of the metabolite inosine (56–58), and Bifidobacteria, among other commensals, is positively associated with responses to cancer immunotherapy in humans (59, 60). Overall, several studies suggest that Bifidobacteria possess immune-stimulating properties in multiple contexts. Our work adds to this by showing that diet-induced enrichment in acetate-producing Bifidobacteria enhances immunological memory against secondary infections.

The question of how DR directly (independently of Bifidobacteria and acetate) enhances the ability of memory T cells to produce cytokines and chemokines during DR remains an open question. Although several elegant studies have demonstrated that acetate

can directly enhance T cell function in various settings (43–46), our data in the context of DR suggest that memory T cell enhancement occurs independently of acetate or Bifidobacteria. Acetate was found to enhance immune cells during DR, but this potentially occurred via its action on myeloid cells. Our findings partially contrast with a recent study, which proposed that Bifidobacteria-derived acetate directly promoted primary T cell responses against MC38 adenocarcinoma in the context of restricted dietary intake. As such, DR may regulate T cell responses against infections and tumors via distinct mechanisms. Further, and not mutually exclusively, DR may differentially impact primary and secondary T cell responses. In the setting of a secondary infection, it could be that DR enhances memory T cell function by directly regulating their metabolic state to promote catabolic processes, which has been linked to optimal development and function of memory T cells (61, 62). Alternatively, but not mutually exclusively, DR may induce host-derived factors that act on memory T cells. For example, DR is known to promote an increase in several factors, including hormones such as glucocorticoids, which have been shown to have immune-enhancing effects in defined contexts (63). Future studies addressing how nutritional interventions enhance distinct immune compartments will be critical to develop rational nutritional interventions for the prevention and treatment of disease.

Materials and Methods

Mice. C57BL/6Tac mice were purchased from Taconic Farms and CD45.1$^+$CD45.2$^+$ mice on a C57BL/6 background were obtained through the NIAID Taconic exchange program (segmented filamentous bacteria positive). YopE-I transgenic mice were generated and bred in house. Female mice were 6 to 8 wk of age at the beginning of each experiment. Germ-free and colonized germ-free C57BL/6 mice were bred and maintained at the NIAID Microbiome Program Gnotobiotic Animal Facility. All mice were bred and maintained under specific pathogen-free conditions at an American Association for the Accreditation of Laboratory Animal Care (AAALAC)-accredited animal facility at the NIAID and housed in accordance with the procedures outlined in the Guide for the Care and Use of Laboratory Animals. Experiments were performed under an animal study proposal (LHIM-2E) approved by the NIAID Animal Care and Use Committee.

Bacteria. Wild-type or mutant *Y. pseudotuberculosis* (32777) strains were grown from bacterial culture in 2XYT media at 25 °C overnight shaking at 200 rpm. Mice were infected with 1×10^7 colony-forming units (CFU) of *Yptb* ΔyopM via oral gavage (mice were fasted overnight prior to oral infection). For secondary infections, mice were injected i.v. with 2×10^2 CFU of WT *Yptb,* and bacterial burden was assessed in the spleen 48 h later. Bacterial burden was determined by serial plating on MacConkey plates, and colonies were counted after incubation at room temperature (RT) for 48 h.

The wild mouse community consists of the following bacterial commensals isolated from fecal samples of wild or "wildling" mice (31, 32). Members include *Olsenella umbonata, Parabacteroides distasonis, Clostridium innocuum, Enterococcus hirae, Faecalibaculum rodentium, Lactobacillus johnsonii, Lactobacillus intestinalis, Veillonella criceti, Pasteurella caecimuris, Rodentibacter heylii*. In these experiments, 6-wk-old male and female germ-free mice were colonized with the abovementioned wild mouse community (lacking Bifidobacteria) via oral gavage. After 4 wk, these mice were used as breeders. After weaning (3 wk of age), half the offspring were moved to a separate isolator and received a combination of *Bifidobacterium longum* subsp.longum 2-2B Biodefense and Emerging Infections Research Resources Repository (BEI resources) and *Bifidobacterium animalis* (isolated from wildling mice) by oral gavage on 2 consecutive days to generate groups of mice containing the wild mouse community with or without Bifidobacteria.

Mouse isolates were grown separately then combined as a defined community prior to oral gavage of breeders. Ten microliters of each frozen strain were propagated either on Columbia agar with 5% sheep blood (Thermo Scientific) or CDC anaerobe 5% sheep blood agar (BD BBL) and incubated under anaerobic conditions, except for *Rodentibacter heylii,* which was grown in aerobic conditions. Colonies were used as start inoculum (OD_{600nm} = 0.01) for liquid cultures. Cultures were incubated under appropriate conditions until OD_{600nm} reached 1. Glycerol stocks of each strain were preserved at −80 °C. To prepare bacterial mix for germ-free mice oral gavage, equal volumes of preserved stocks were pooled under anaerobic conditions, centrifuged, and resuspended in prereduced PBS.

Dietary Restriction. From this, we found that individual female and male mice consumed 2.75 grams and 3.4 grams of food per day, respectively, consistent with previous reports (64). As such, we provided 1.375 g of food to female mice (5.7 kcal per day) and 1.7 g to male mice (7.0 kcal) daily to ensure 50% DR. Mice on DR consumed all the food provided. For fiber studies, mice received a diet with 10% inulin and 5% cellulose (Teklad custom diet, TD.210347), or an isocaloric diet with only 5% cellulose (Teklad custom diet, TD.130654) either ad libitum or at 50% restriction at the memory phase.

Tissue Processing and Flow Cytometry. Mice were killed with CO_2. Tissues were harvested and placed in cold phosphate buffered saline (PBS). Spleen and lymph nodes were processed through a 70-μM filter. Cells were stained for flow cytometry for 15 to 30 min in PBS on ice. Antibodies for flow cytometry were purchased from eBioscience, Becton Dickinson (BD) Pharmingen or Biolegend unless otherwise noted, and were conjugated to Pacific Blue, BV605, BV785, BV510, BV650, eFluor 450, APC, AlexaFluor 647, Pe-Texas Red, PE-CF594, FITC, PE, PerCPCy5.5, PECy7, APCCy7, APCe780, PerCPe710, BV421, or Alexa Flour 700. DAPI or Live/Dead fixable stain (Life Technologies) was used to identify dead cells in all experiments. Intracellular staining for chemokine- and cytokine-producing cells was performed using a BD intracellular staining kit or the eBiosciences FOXP3 staining kit. To determine cytokine and chemokine production in T cells, cells were stimulated with phorbol myristate acetate (50 ng/mL), ionomycin (1 mM), and BD GolgiPlug (BFA) (1 μL/mL) for 2.5 h at 37 °C before staining for flow cytometry. To detect cytokines in myeloid cells, they were incubated with BFA (1 μL/mL) alone for 2.5 h at 37 °C before staining for flow cytometry. The following antibodies were used for staining of murine cells: CD4 (RM4-5), CD8b (H35-17.2), FOXP3 (FJK-16S), IFN-γ (XMG1.2), CD45 (30-F11), CD45.1 (A20), CD45.2 (104), CD90.2 (30-H12), TCRβ (H57-597), CD44 (IM7), NK1.1 (PK136), γδTCR (GL3), B220 (RA3-6B2), CD11b (M1/70), CD11c (N418), MHC-II (M5/114,15.2), Ly-6C (HK1.4), Ly-6G (clone 1A8), IL-2 (JES6-5H4), CCL5 (2E9), IL-1β (NJTEN3), TNFα (MP6-XT22), CCL3 (purified polyclonal goat, R&D Systems), CCL4 (purified polyclonal goat, R&D Systems), and XCL1 (purified polyclonal goat, R&D Systems). A rabbit anti-goat IgG (H+L) secondary antibody conjugated to AlexaFluor 647 (Thermofisher) was used to detect purified antibodies. To detect YopE-specific CD8$^+$ T cells using a tetramer, we used a PE-labeled tetramer provided by the NIH Tetramer Core Facility. All staining contained purified anti-CD16/32 to block nonspecific Fc receptor binding (2.4G2, BioXcell). Cells were acquired on a BD Fortessa X-20 flow cytometer, and data were analyzed using FlowJo software (TreeStar). Cells were sorted on a MA900 cell sorter (Sony) with a 100-μm chip.

In Vivo Acetate Supplementation. Similar to what has been described (43), mice received drinking water supplemented with 200 mM acetate the day prior to the secondary infection and until the end of the experiment (72 h in total). Mice also received an i.p. injection of sodium acetate (500 mg/kg) on days 0 and 1 of the secondary infection.

RNA Sequencing. 20,000 inflammatory monocytes (CD11b$^+$ Ly6C$^+$ Ly6G$^-$) and neutrophils (CD11b$^+$ Ly6g$^+$) were sorted from the spleen of mice fed ad libitum and on DR at 9 h post a secondary infection with *Yptb*. As has been described (65), RNA from sorted cells was extracted using the RNeasy Plus Micro Kit (Qiagen) as per manufacturer instructions. Libraries were prepared using the Clontech SMARTer Ultra low input mRNA-Seq sequence kit, and samples were sequenced paired end (100 bp paired end) on a NextSeq550. For analysis, RNA-seq samples were mapped to the mm10 mouse genome with STAR.77. Gene expression was assessed using HOMER's analyzeRepeats.pl with parameters rna, mm10, -count exons, -condenseGenes. The GEO accession number is GSE242696.

16S rRNA Gene Profiling. As described (66), DNA was extracted from fecal pellets using phenol:chloroform or the MagAttract PowerMicrobiome DNA/RNA Kit. 16S V4 rDNA libraries were prepared using the Phusion High-Fidelity PCR Master Mix with primers 515F and 806R, and sequenced on an Illumina MiSeq instrument by the NIAID Microbiome Program core facility. 16S data were analyzed using QIIME 2 (v2020.2). Briefly, reads were denoised using the q2-dada2 plugin (exact

parameters were forward reads truncated to 240 bases with 20 bases trimmed from the 5′ end, reverse reads truncated to 150 bases with 20 bases trimmed from the 5′ end, and bases truncated with quality score below 10). Using the q2-feature-table plugin, samples were rarefied to the depth of the sample with the fewest reads (>20,000 reads), and sequence variants were filtered if they did not occur in at least 4 samples. Rooted phylogenetic trees were generated using the align-to-tree-mafft-fasttree method in the q2-phylogeny plugin. Alpha and beta diversity analyses were performed using the core-metrics-phylogenetic method in the q2-diveristy plugin, with a sampling depth of 10,000 reads. Taxonomy was assigned to sequence variants using the q2-feature-classifier plugin and a naive Bayes classifier pretrained on the SILVA 132 515F/806R 99% OTUs provided as a QIIME 2 data resource. A pseudocount of 1 was applied prior to calculating the fold change in the relative abundance of each taxonomic group. Significance was calculated using a custom R script to perform the Mann–Whitney *U* test for each taxonomic group.

Shotgun Metagenomics. Metagenomics libraries were generated using the Illumina DNA Prep kit, with 500 ng purified DNA as template, and sequenced on an Illumina NextSeq instrument by the NIAID Microbiome Program core facility. Metagenomics data were analyzed on the NIH HPC Biowulf cluster (https://hpc.nih.gov/). Briefly, reads were first processed using KneadData (http://huttenhower.sph.harvard.edu/kneaddata) to remove contaminants (reads derived from the mouse genome or bacterial 16S rRNA gene). KneadData was used with default parameters except for including the option of removing tandem repeats. Per sample, KneadData generates four output files (pair 1 reads, pair 2 reads, unmatched pair 1 reads, and unmatched pair 2 reads). These four files were concatenated into a single file for each sample and then analyzed using HUMAnN 3.0 to profile metabolic pathways (67). HUMAnN version 3.0.0-alpha.3 was used with default parameters; the version of the ChocoPhlAn and UniRef90 databases was 201901; the dependency versions were Python v3.8, Bowtie2 v2.4.2, and DIAMOND v2.0.4. The output pathway abundance table for each sample was then normalized to copies per million using the humann_renorm_table script, and once normalized, these abundance tables were joined into a single table using the humann_join_tables script. Finally, a pseudocount of 1 was applied to the joined abundance table prior to calculating the fold change in the relative abundance of each metabolic pathway. Significance was calculated using a custom R script to perform the Mann–Whitney *U* test for each metabolic pathway.

FAST-ATAC-Seq. FAST-ATAC-seq was performed as previously described (68). Briefly, 10,000 splenic YopE-I cells or bone marrow monocytes or neutrophils were sorted and pelleted by centrifugation at 500 g for 5 min at 4 °C. Supernatant was removed, and cell pellets were resuspended in 45 μL of transposase mixture (25 μL of Tagment DNA buffer, 2.5 μL of Tagment DNA enzyme, 0.5 μL of 1% digitonin, and 17 μL of H_2O) and incubated for 30 min at 37 °C with agitation at 300rpm. Tagmented DNA was purified using the QIAGEN MinElute Reaction Cleanup Kit, and purified DNA was eluted in 10 μL of elution buffer. Tagmented fragments were amplified with 10 to 15 PCR cycles on the basis of an amplification curve. After purification using the QIAGEN PCR cleanup kit, samples were sequenced single end on a NextSeq 550 (Illumina). ATAC-seq reads were mapped with STAR to the mm10 reference genome with default parameters. Peaks were called using HOMER's findPeaks with parameters. Next, irreproducible discover rate was run, and only peaks that were found in at least two samples were considered for further downstream analysis. Motif enrichment analysis was performed using HOMER's findMotifsGenome.pl with standard parameters. For pathway analysis, ATAC peaks were replaced by the name of the nearest gene. After differential expression testing, each gene had a fold change and associated *P* values. Fold changes with associated genes were ranked for GSEA testing using the clusterProfiler package (https://www.sciencedirect.com/science/article/pii/S2666675821000667). GSEA testing was used to find pathways (with genes) that are significantly overrepresented in the up-regulated or down-regulated region of the ranking. emaplot was used to plot out the top 50 significant pathways (size reflects the number of genes in that pathway), and color indicates the significance level) (http://yulab-smu.top/biomedical-knowledge-mining-book/enrichplot.html). Each dot represents a pathway item (GO biological function), and a line connecting two dots represents sharing of member genes between two pathways. Each dot in the graph represents a significant outcome from a GSEA test. For each GSEA test, all the genes in the expression profile were used, and these genes were ranked by fold-changes (DR versus control). GSEA testing takes this ranking as input and tests against a pathway in the GO biological function database to check whether the members of that pathway are preferentially found in the upstream (upregulation) or downstream (downregulation) of the ranking.

Generation of *Y. pseudotuberculosis*–Specific Transgenic Mice (YopE-I Mice). Wild-type C57BL/6 mice were infected with ΔyopM Yptb via oral gavage. At day 7 post infection, $CD8^+$ T cells that bound a tetramer recognizing $CD8^+$ T cells specific for the immunodominant YopE antigen of *Yptb* (NIH tetramer core) (35) were FACSorted from mesenteric lymph nodes and subjected to single-cell sequencing of TCRα and TCRβ chains. Clonal TCR pairs were identified and used in a hybridoma reconstitution screening assay to identify *Yptb*-reactive TCR heterodimers. A single *Yptb*-specific TCR pair was cloned into a hCD2-expression vector and used to generate TCR-transgenic mice (YopE-I), to track *Yptb*-specific $CD8^+$ T cells in vivo.

Adoptive Transfer of *Y. pseudotuberculosis*–Specific $CD8^+$ T Cells (YopE-I Cells). 10^5 YopE-I $Rag1^{-/-}$ $CD8^+$ T cells were transferred to $CD45.2^+$ or $CD45.1^+$ $CD45.1^+$ recipient mice by retro-orbital intravenous injection 1 d prior to infection with *Yptb*.

Gentamycin Killing Assay. Mature monocytes and neutrophils were purified from bone marrow of mice fed ad libitum or on DR. A 2:1 ratio of neutrophils:-monocytes (1×10^6 total) were co-cultured with 1×10^7 WT *Yptb* (MOI = 10) for 1 h at 37 °C, allowing cells to internalize *Yptb*. Gentamicin (100 μg/mL) was added to the culture to kill extracellular *Yptb*. Two hours after adding gentamicin, cells were harvested, spun down, and resuspended in 200 μL of 1% Triton-X for 2 min to lyse the cells and release intracellular *Yptb*. Then, 800 μL of PBS was added, and serial dilutions were made and plated on MacConkey plates. Experimental groups included cells treated with 20 ng/mL IFNγ alone, 1 mM acetate alone, the combination of IFNγ and acetate, or just media. IFNγ and acetate were present in cultures throughout the experiment (i.e., added at the same time as *Yptb*).

Measurement of Short-Chain Fatty Acids. Serum was obtained from mice fed ad libitum or on DR for 4 wk. To measure short-chain fatty acids, LC-MS analysis was performed in duplicate on a Thermo Vanquish UPLC–Thermo Altis triple quadrupole mass spectrometer.

Quantification and Statistical Analysis. Groups were compared with Prism V8 software (GraphPad) using a two-tailed Mann–Whitney *U* test. Differences were considered to be statistically significant when $P < 0.05$. $*P < 0.05$, $**P < 0.01$, $***P < 0.001$, $****P < 0.0001$; ns, not significant. Sample sizes were determined based on previous experience with similar experiments.

Data, Materials, and Software Availability. The datasets generated during this study can be found using the GEO accession number GSE242696 (37). All other data are included in the manuscript and/or *SI Appendix*.

ACKNOWLEDGMENTS. Y.B. is supported by the Division of Intramural Research of National Institute of Allergy and Infectious Diseases (NIAID) (1ZIAAI001132, 1ZIAAI001115, and 1ZICAI001233 to Y.B.), NIH. N.C. is supported by R00CA252443 (National Cancer Institute, NIH) and The Feldstein Medical Foundation. We thank the Belkaid lab for their suggestions, support, and critical reading of the manuscript. We would like to thank K. Beacht, E. Lewis, A. and G. Koroleva for technical assistance, the NIAID animal facility staff, and Yunhua Zhu for bioinformatics analysis.

Author affiliations: [a]Metaorganism Immunity Section, Laboratory of Host Immunity and the Microbiome, National Institute of Allergy and Infectious Diseases, NIH, Bethesda, MD 20892; and [b]Department of Integrative Biology and Physiology, University of California, Los Angeles, CA 90095

Author contributions: S.-J.H., Y.B., and N.C. designed research; S.-J.H., A.S., D.C., M.K.D.S., A.T., D.S.Y., P.J.P.-C., N.B., A.I.L., M.E., and N.C. performed research; S.-J.H., A.S., V.M.L., L.C., and N.C. analyzed data; and Y.B. and N.C. wrote the paper.

Reviewers: C.A.H., University of Pennsylvania; and D.L.K., Harvard Medical School.

The authors declare no competing interest.

1. N. Collins, Y. Belkaid, Control of immunity via nutritional interventions. *Immunity* **55**, 210–223 (2022).
2. N. Collins, Dietary regulation of memory T cells. *Int. J. Mol. Sci.* **21**, 4363 (2020).
3. C. Wilhelm, J. Surendar, F. Karagiannis, Enemy or ally? Fasting as an essential regulator of immune responses. *Trends Immunol.* **42**, 389–400 (2021).
4. A. H. Lee, V. D. Dixit, Dietary regulation of immunity. *Immunity* **53**, 510–523 (2020).
5. D. Zeevi *et al.*, Personalized nutrition by prediction of glycemic responses. *Cell* **163**, 1079–1094 (2015).
6. N. Collins *et al.*, The bone marrow protects and optimizes immunological memory during dietary restriction. *Cell* **178**, 1088–1101.e1015 (2019).
7. C. Palma *et al.*, Caloric restriction promotes immunometabolic reprogramming leading to protection from tuberculosis. *Cell Metab.* **33**, 300–318.e312 (2021).
8. S. Jordan *et al.*, Dietary intake regulates the circulating inflammatory monocyte pool. *Cell* **178**, 1102–1114.e1117 (2019).
9. Y. Q. Mao *et al.*, The antitumour effects of caloric restriction are mediated by the gut microbiome. *Nat. Metab.* **5**, 96–110 (2023).
10. E. C. Lien *et al.*, Low glycaemic diets alter lipid metabolism to influence tumour growth. *Nature* **599**, 302–307 (2021).
11. S. Brandhorst *et al.*, A periodic diet that mimics fasting promotes multi-system regeneration, enhanced cognitive performance, and healthspan. *Cell Metab.* **22**, 86–99 (2015).
12. S. Brandhorst, V. D. Longo, Fasting and caloric restriction in cancer prevention and treatment. *Recent Results Cancer Res.* **207**, 241–266 (2016).
13. I. Caffa *et al.*, Fasting-mimicking diet and hormone therapy induce breast cancer regression. *Nature* **583**, 620–624 (2020).
14. I. Y. Choi *et al.*, A diet mimicking fasting promotes regeneration and reduces autoimmunity and multiple sclerosis symptoms. *Cell Rep.* **15**, 2136–2146 (2016).
15. A. N. Crupi, J. Haase, S. Brandhorst, V. D. Longo, Periodic and intermittent fasting in diabetes and cardiovascular disease. *Curr. Diab. Rep.* **20**, 83 (2020).
16. S. Di Biase *et al.*, Fasting-mimicking diet reduces HO-1 to promote T cell-mediated tumor cytotoxicity. *Cancer Cell* **30**, 136–146 (2016).
17. C. Lee *et al.*, Fasting cycles retard growth of tumors and sensitize a range of cancer cell types to chemotherapy. *Sci. Transl. Med.* **4**, 124ra127 (2012).
18. M. P. Mattson, V. D. Longo, M. Harvie, Impact of intermittent fasting on health and disease processes. *Ageing Res. Rev.* **39**, 46–58 (2017).
19. G. Salvadori, M. G. Mirisola, V. D. Longo, Intermittent and periodic fasting, hormones, and cancer prevention. *Cancers (Basel)* **13**, 4587 (2021).
20. J. L. Sonnenburg, F. Backhed, Diet-microbiota interactions as moderators of human metabolism. *Nature* **535**, 56–64 (2016).
21. E. Ansaldo, T. K. Farley, Y. Belkaid, Control of immunity by the microbiota. *Annu. Rev. Immunol.* **39**, 449–479 (2021).
22. A. F. Salvador, K. A. de Lima, J. Kipnis, Neuromodulation by the immune system: A focus on cytokines. *Nat. Rev. Immunol.* **21**, 526–541 (2021).
23. E. D. Sonnenburg, J. L. Sonnenburg, The ancestral and industrialized gut microbiota and implications for human health. *Nat. Rev. Microbiol.* **17**, 383–390 (2019).
24. J. L. Sonnenburg, E. D. Sonnenburg, Vulnerability of the industrialized microbiota. *Science* **366**, eaaw9255 (2019).
25. S. P. Spencer, G. K. Fragiadakis, J. L. Sonnenburg, Pursuing human-relevant gut microbiota-immune interactions. *Immunity* **51**, 225–239 (2019).
26. S. Fabbiano *et al.*, Functional gut microbiota remodeling contributes to the caloric restriction-induced metabolic improvements. *Cell Metab.* **28**, 907–921.e907 (2018).
27. F. Cignarella *et al.*, Intermittent fasting confers protection in CNS autoimmunity by altering the gut microbiota. *Cell Metab.* **27**, 1222–1235.e1226 (2018).
28. G. S. Hotamisligil, Inflammation, metaflammation and immunometabolic disorders. *Nature* **542**, 177–185 (2017).
29. E. D. Sonnenburg *et al.*, Diet-induced extinctions in the gut microbiota compound over generations. *Nature* **529**, 212–215 (2016).
30. P. J. Turnbaugh *et al.*, An obesity-associated gut microbiome with increased capacity for energy harvest. *Nature* **444**, 1027–1031 (2006).
31. S. P. Rosshart *et al.*, Laboratory mice born to wild mice have natural microbiota and model human immune responses. *Science* **365**, eaaw4361 (2019).
32. S. P. Rosshart *et al.*, Wild mouse gut microbiota promotes host fitness and improves disease resistance. *Cell* **171**, 1015–1028.e1013 (2017).
33. L. K. Beura *et al.*, Normalizing the environment recapitulates adult human immune traits in laboratory mice. *Nature* **532**, 512–516 (2016).
34. J. D. Lin *et al.*, Rewilding Nod2 and Atg16l1 mutant mice uncovers genetic and environmental contributions to microbial responses and immune cell composition. *Cell Host. Microbe.* **27**, 830–840.e834 (2020).
35. S. J. Han *et al.*, White adipose tissue is a reservoir for memory t cells and promotes protective memory responses to infection. *Immunity* **47**, 1154–1168.e1156 (2017).
36. D. M. Fonseca *et al.*, Microbiota-dependent sequelae of acute infection compromise tissue-specific immunity. *Cell* **163**, 354–366 (2015).
37. S.-J. Han *et al.*, Sequencing data for: Microbiota configuration determines nutritional immune optimization. Gene expression Omnibus (GEO). https://www.ncbi.nlm.nih.gov/geo/query/acc.cgi?acc=GSE242696. Deposited 25 January 2023.
38. N. Arpaia *et al.*, Metabolites produced by commensal bacteria promote peripheral regulatory T-cell generation. *Nature* **504**, 451–455 (2013).
39. S. Fukuda *et al.*, Bifidobacteria can protect from enteropathogenic infection through production of acetate. *Nature* **469**, 543–547 (2011).
40. K. M. Maslowski *et al.*, Regulation of inflammatory responses by gut microbiota and chemoattractant receptor GPR43. *Nature* **461**, 1282–1286 (2009).
41. S. Fukuda, H. Toh, T. D. Taylor, H. Ohno, M. Hattori, Acetate-producing bifidobacteria protect the host from enteropathogenic infection via carbohydrate transporters. *Gut Microbes* **3**, 449–454 (2012).
42. Z. T. Schug, J. Vande Voorde, E. Gottlieb, The metabolic fate of acetate in cancer. *Nat. Rev. Cancer* **16**, 708–717 (2016).
43. M. L. Balmer *et al.*, Memory CD8(+) T cells require increased concentrations of acetate induced by stress for optimal function. *Immunity* **44**, 1312–1324 (2016).
44. J. Qiu *et al.*, Acetate promotes T cell effector function during glucose restriction. *Cell Rep.* **27**, 2063–2074.e2065 (2019).
45. R. D. Leone *et al.*, Glutamine blockade induces divergent metabolic programs to overcome tumor immune evasion. *Science* **366**, 1013–1021 (2019).
46. S. K. Vodnala *et al.*, T cell stemness and dysfunction in tumors are triggered by a common mechanism. *Science* **363**, eaau0135 (2019).
47. J. L. Fachi *et al.*, Acetate coordinates neutrophil and ILC3 responses against *C. difficile* through FFAR2. *J. Exp. Med.* **217**, jem.20190489 (2020).
48. M. G. Machado *et al.*, Acetate improves the Killing of *Streptococcus pneumoniae* by alveolar macrophages via NLRP3 inflammasome and glycolysis-HIF-1alpha axis. *Front. Immunol.* **13**, 773261 (2022).
49. D. Erny *et al.*, Microbiota-derived acetate enables the metabolic fitness of the brain innate immune system during health and disease. *Cell Metab.* **33**, 2260–2276.e2267 (2021).
50. A. Al-Roub *et al.*, Short chain fatty acid acetate increases TNFalpha-induced MCP-1 production in monocytic cells via ACSL1/MAPK/NF-kappaB axis. *Int. J. Mol. Sci.* **22**, 7683 (2021).
51. C. N. Spencer *et al.*, Dietary fiber and probiotics influence the gut microbiome and melanoma immunotherapy response. *Science* **374**, 1632–1640 (2021).
52. A. Trompette *et al.*, Dietary fiber confers protection against Flu by shaping Ly6c(-) patrolling monocyte hematopoiesis and CD8(+) T cell metabolism. *Immunity* **48**, 992–1005.e1008 (2018).
53. Q. Y. Ang *et al.*, Ketogenic diets alter the gut microbiome resulting in decreased intestinal Th17 cells. *Cell* **181**, 1263–1275 e1216 (2020).
54. H. C. Wastyk *et al.*, Gut-microbiota-targeted diets modulate human immune status. *Cell* **184**, 4137–4153.e4114 (2021).
55. S. Fushinobu, Unique sugar metabolic pathways of bifidobacteria. *Biosci. Biotechnol. Biochem.* **74**, 2374–2384 (2010).
56. A. Sivan *et al.*, Commensal Bifidobacterium promotes antitumor immunity and facilitates anti-PD-L1 efficacy. *Science* **350**, 1084–1089 (2015).
57. L. F. Mager *et al.*, Microbiome-derived inosine modulates response to checkpoint inhibitor immunotherapy. *Science* **369**, 1481–1489 (2020).
58. S. H. Lee *et al.*, Bifidobacterium bifidum strains synergize with immune checkpoint inhibitors to reduce tumour burden in mice. *Nat. Microbiol.* **6**, 277–288 (2021).
59. V. Matson *et al.*, The commensal microbiome is associated with anti-PD-1 efficacy in metastatic melanoma patients. *Science* **359**, 104–108 (2018).
60. K. A. Lee *et al.*, Cross-cohort gut microbiome associations with immune checkpoint inhibitor response in advanced melanoma. *Nat. Med.* **28**, 535–544 (2022).
61. K. Araki *et al.*, mTOR regulates memory CD8 T-cell differentiation. *Nature* **460**, 108–112 (2009).
62. X. Xu *et al.*, Autophagy is essential for effector CD8(+) T cell survival and memory formation. *Nat. Immunol.* **15**, 1152–1161 (2014).
63. A. Shimba *et al.*, Glucocorticoids drive diurnal oscillations in T cell distribution and responses by inducing Interleukin-7 receptor and CXCR4. *Immunity* **48**, 286–298.e286 (2018).
64. V. A. Acosta-Rodriguez, M. H. M. de Groot, F. Rijo-Ferreira, C. B. Green, J. S. Takahashi, Mice under caloric restriction self-impose a temporal restriction of food intake as revealed by an automated feeder system. *Cell Metab.* **26**, 267–277.e262 (2017).
65. M. Enamorado *et al.*, Immunity to the microbiota promotes sensory neuron regeneration. *Cell* **186**, 607–620.e17 (2023).
66. A. Stacy *et al.*, Infection trains the host for microbiota-enhanced resistance to pathogens. *Cell* **184**, 615–627.e617 (2021).
67. F. Beghini *et al.*, Integrating taxonomic, functional, and strain-level profiling of diverse microbial communities with bioBakery 3. *Elife* **10**, e65088 (2021).
68. A. I. Lim *et al.*, Prenatal maternal infection promotes tissue-specific immunity and inflammation in offspring. *Science* **373**, eabf3002 (2021).